Pickering emulsion droplets and solid microspheres acting synergistically for continuous-flow cascade reactions

names and address needed

…. B.P. Binks[b]

[b]*Department of Chemistry, University of Hull, Hull. HU6 7RX. UK*

*Corresponding author: hqyang@sxu.edu.cn

Submitted to: Nature Catalysis on ?.3.23

Contains Supplementary Information

Abstract

Efficient integration of multiple incompatible reactions in one reaction system is of paramount significance for green synthetic chemistry. However, this goal is extremely challenging to achieve especially under industrially preferred continuous-flow conditions. Herein, we develop a conceptually novel method, by co-packing micron-sized Pickering emulsion droplets (PEDs) and solid microspheres (SMs) in one column reactor. The PEDs and SMs co-packed system can not only provide the favorite microenvironments for each incompatible catalyst but also enable them to work synergistically through directional transfer of reaction intermediates from SMs to PEDs. The success of the concept is based on a phenomenon found here, namely coexistence of droplets and solid microspheres without droplet disruption even under flow and high pressure due to specific interactions. As proof of concept, two chemo-enzymatic cascade reactions for continuous synthesis of chiral cyanohydrins and chiral esters were examined, which both exhibited 7 to 77-fold enhanced cascade reaction efficiency (in comparison to the batch and continuous-flow counterparts), 99% enantioselectivity and long-term operational stability (240 h). Our method would significantly widen the concept of conventional fixed-bed catalysis, providing an efficient platform for continuous-flow cascade catalysis even involving incompatible homogeneous, heterogeneous and biological catalysts.

Introduction

Cascading of multiple catalytic reactions in one reaction system is of significance for green synthetic chemistry owing to several appealing advantages such as avoidance of separation of the intermediate and generation of beneficial thermodynamic/kinetic coupling effects[1-4]. However, realization of efficient cascade catalysis is very challenging because of the difficulty in exquisite integration of multiple catalysts together ensuring spatiotemporal coupling[5]. More challenging is the efficient integration of categorically different heterogeneous, homogeneous and biological catalysts in industrially desired continuous-flow fashion since homogeneous or biological catalysts often require a special liquid phase medium[6-12]. Although various methods have been explored to construct continuous-flow cascade catalysis, such as physical mixing of two or more catalyst types[13,14], multi-layering of different catalyst types[15,16] or two-stage reactions linked in series in fixed-bed reactors[17-19], these systems are largely limited to conventional heterogeneous catalytic systems and are not adaptable to those cascade systems involving homogenous and biological catalysts[7].

The key to the realization of an efficient integration of homogenous or biological catalysts with heterogeneous ones is to create their own liquid microenvironments, ensuring that the different catalysts can work efficiently and cooperatively in continuous-flow systems[20-23]. Recently, we developed Pickering emulsion droplet-based continuous-flow reaction systems, in which micron-sized droplets harboring homogeneous catalysts or enzymes were packed in a column reactor in the same way as solid particle catalysts pack in fixed-bed reactors[24-26]. Due to the high stability to coalescence of Pickering emulsion droplets, the continuous-flow systems work efficiently with reactants continuously fed into the reactor and products collected from the reactor, while the homogeneous catalysts or enzymes are retained in the fixed-bed reactor as a result of the

confinement of droplets. We and others have demonstrated that this droplet-based continuous-flow system could provide a vast opportunity to continuous utilization of homogeneous and biological catalysts[24-30], owing to several critical merits including a high flexibility in choosing liquids to prepare Pickering emulsion droplets, good capability of the droplets to confine homogeneous or biological catalysts and excellent ability in controlling reactions at a nanometer-to-micrometer scale[31-37]. We hypothesize that if we are able to co-pack Pickering emulsion droplets (PEDs) and solid microspheres (SMs) in a column reactor and further enable them to work cooperatively, efficient cascading of homogeneous, heterogeneous and biological systems for continuous-flow reactions would be possible.

Figure 1a schematically presents our concept of a novel continuous-flow cascade system, which is constructed by co-packing ionic liquid (IL) droplet-based PEDs and SMs in oil in a column reactor. This concept is based on a phenomenon found concerning the significant enhancement in the stability of PEDs in the presence of SMs because of their mutual interactions. Due to the presence of different micro-compartmentalized environments and the nanoscale distances between PEDs and SMs, our system allows for integration of incompatible homogeneous catalysts, enzymes and heterogeneous catalysts and can work synergistically for cascade reactions. We showcase use of our concept to conduct two chemo-enzymatic cascade continuous-flow reactions for the synthesis of chiral cyanohydrins and chiral esters, obtaining 7 to 77-fold enhancement in the cascade efficiency, 99% enantiomeric excess as well as good durability not achievable with existing methods. The mechanism of how PEDs and SMs work synergistically is proposed.

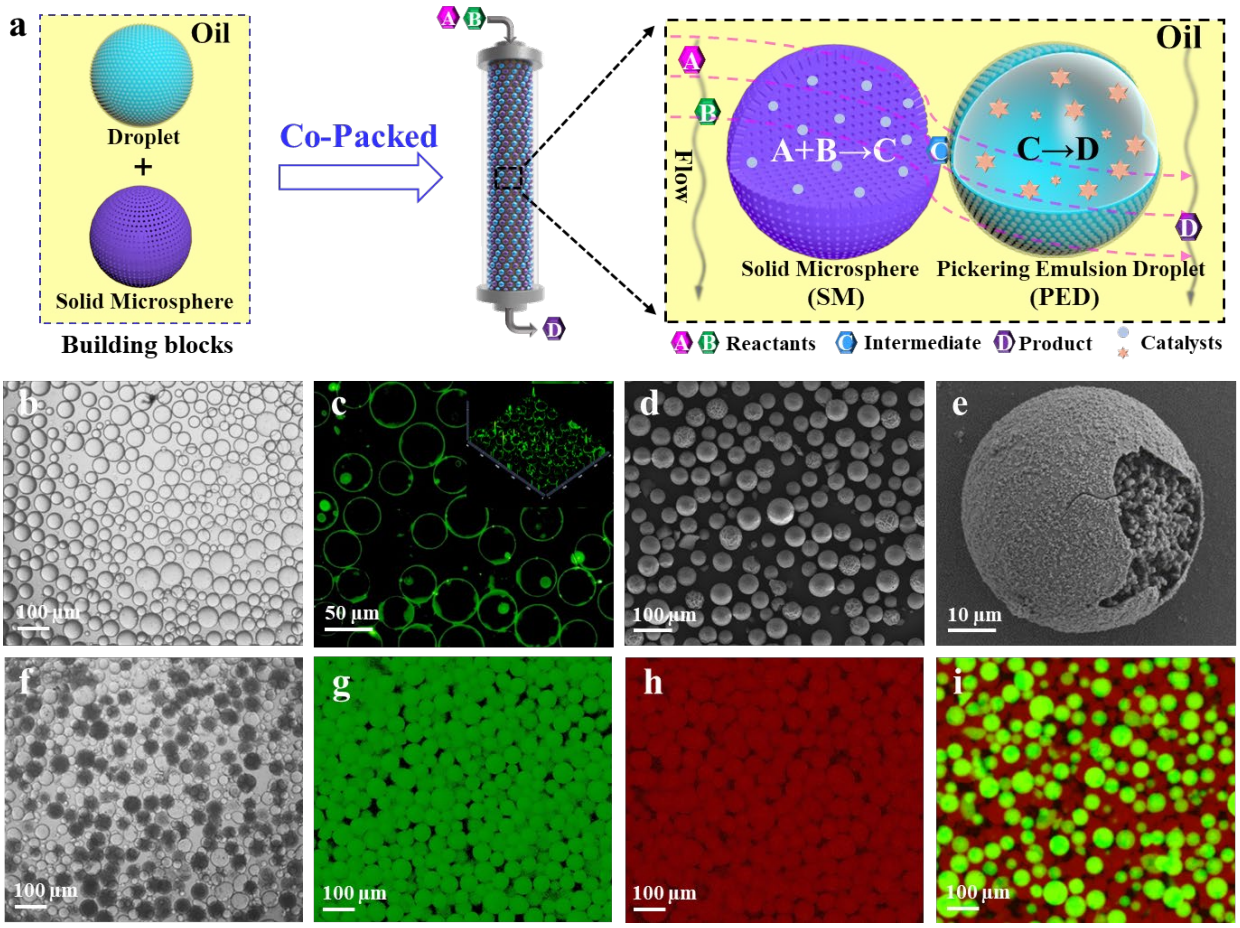

Fig. 1 | Illustration of PEDs and SMs co-packed in bed reactor and coexistence of PEDs and SMs. a Schematic illustration of the concept**. b** Optical micrograph of an IL-in-oil Pickering emulsion. **c** CLSM image of PEDs with the emulsifier dyed by FITC-I. **d** SEM image of SMs. **e** Magnified SEM of a SM showing the interior structure. **f** Optical micrograph of a mixture of PEDs and SMs. **g** CLSM image of FITC-I-labelled SMs. **h** CLSM image of PEDs with IL dyed by RBITC. **i** CLSM image of a mixture of RBITC-labelled PEDs and FITC-I-labelled SMs. All Pickering emulsions are composed of 2 mL IL, 1 mL *n*-octane and 0.06 g silica particle emulsifier.

Results

Enhanced stability of Pickering emulsion droplets in the presence of solid microspheres. An ionic liquid (IL) was chosen here to prepare Pickering emulsion droplets because ILs can be molecularly designed to not only allow dissolution/dispersion of homogeneous catalysts or biocatalysts but in some cases enrich organics from surroundings[38]. Since most reactants are oil-soluble, IL-based droplets in oil were fabricated through emulsification of a biphasic mixture of

[BMIM]PF_6 and *n*-octane in the presence of silica nanoparticles modified with dimethyldichlorosilane (transmission electron microscopy (TEM), N_2 sorption isotherms, Fourier transform infrared (FTIR) spectroscopy, thermogravimetric analysis (TGA) and air–water contact angle are included in Supplementary Figures 1 and 2). Figure 1b displays an optical micrograph of the as-prepared droplets, which present spherical morphology with average diameters of 46 ± 10 μm. Location of the particles of emulsifier at the surface of droplets was confirmed by confocal laser scanning microscopy (CLSM, Figure 1c, the emulsifier particles were labeled with fluorescein isothiocyanate I FITC-I and the methods were provided in Supplementary Methods 3). This irreversible adsorption of solid particles at the IL-oil interface leads to their extreme stability thus rendering them resistant to coalescence. Porous silica microspheres (SMs) synthesized according to our previous method were chosen as particles for loading catalysts, whose sizes are close to the droplet sizes (Supplementary method 3)[39]. As the scanning electron microscopy (SEM) image shows (Figure 1d), the SMs assume a spherical morphology with a particle diameter distribution centered at 48 ± 10 μm. There are numerous uniform small spheres of *ca*. 900 nm and some voids inside SMs. The specific surface area and average pore size of the SMs are as high as 590 $m^2\ g^{-1}$ and 7 nm, respectively (Figure 1e and Supplementary Figure 3). Such a structure is expected to enhance molecular transport[39]. Using PEDs and SMs of micron-size dimensions to pack fixed-bed is expected to favor reactants passing through the column reactor with low pressure drop[40], which is essential for practical applications.

Next, we investigated the possibility of coexistence of PEDs with SMs in one system under flow and pressured conditions. Due to the propensity of liquid spreading at solid surfaces and the interfacial instability of emulsion droplets[40,41], it is difficult to realize the coexistence of emulsion

droplets with solid particles even under static conditions. For example, Supplementary Figure 4 presents a scenario of adding SMs to a surfactant-stabilized emulsion. Droplets were observed to break up after mixing. Surprisingly, in the case of Pickering emulsion droplets, the droplets were observed to retain their initial spherical morphology (Figure 1f). Even after standing for 48 h, the droplets were still stable without any change in morphology. This phenomenon was also observed in a fluorescence-labeling experiment (Figures 1g-i). Both PEDs and SMs remain discrete without any droplet disruption or aggregation (Figure 1i). To evaluate the stability of the mixed system under simulated industrial conditions, we set up a fixed-bed system by packing PEDs and SMs homogeneously in a column reactor (v/v = 1:1), allowing an oil phase to continuously pass through the reactor under pressure (54 mL h^{-1}, 1.3 MPa). To our delight, even after 48 h of continuous-flow, the droplets in the co-packed system remained intact retaining their spherical morphology well (Supplementary Figure 5). In contrast, for the neat Pickering emulsion droplet-based system (in the absence of SMs), the droplets broke up when the applied pressure was above 0.5 MPa (Supplementary Figure 6). These results demonstrate the mechanical robustness of the co-packed system to withstand the flowing liquid under pressurized conditions and also indicates that the presence of SMs is helpful in stabilizing PEDs.

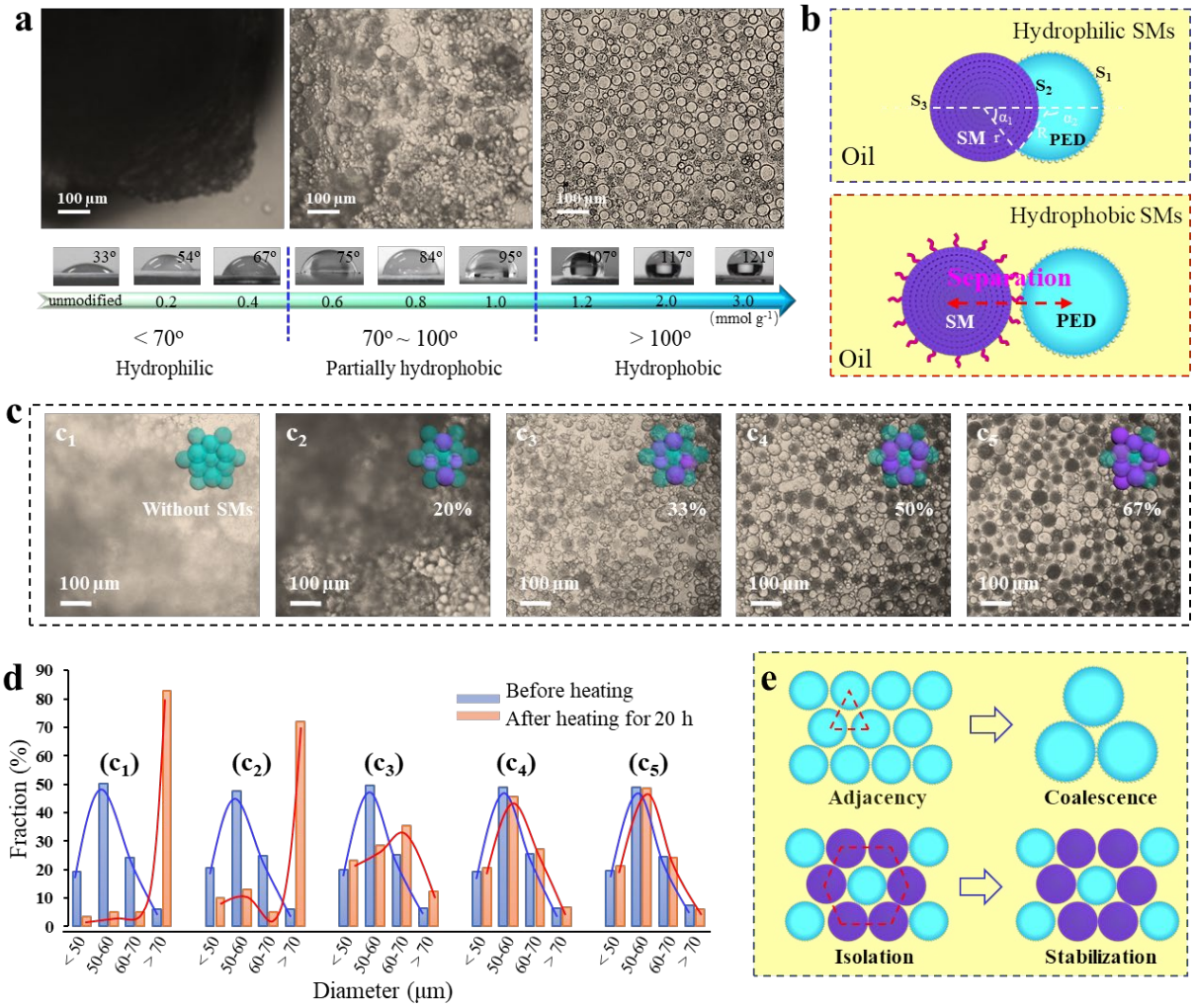

Fig. 2 | Investigation of the interactions between liquid droplets and solid microspheres. a Air-water contact angles of SMs modified with different amounts of *n*-octyltrimethoxysilane and optical micrographs of mixtures of PEDs and SMs of different hydrophobicity. **b** Schematic illustration showing the state of mixing of IL droplets with hydrophilic or hydrophobic SMs. **c** Optical micrographs of mixtures of PEDs with different volume fractions of SMs (with respect to the total volume of mixture, details in Supplementary Figure 10): c_1, without SMs; c_2, 20%; c_3, 33%; c_4, 50%; c_5, 67%. **d** Droplet size distribution of mixed systems c_1-c_5 before and after heating to 120 ºC for 20 h. **e** Schematic illustration of the "isolation" mechanism: Upper-without SMs, lower-with hydrophobic SMs.

a in 70° to 100°, change ~ to –

b labels for R and α_2 not visible

e change Adjaceny to Neighbouring

Origin of the enhanced stability of PEDs in the presence of SMs. We found that the stability of

PEDs in our co-packed system is related to the surface wettability of the SMs. The surface wettability of SMs was finely tuned through surface modification with different doses of *n*-octyltrimethoxysilane (from 0.2 to 3 mmol g^{-1}). Unmodified SMs are quite hydrophilic since the air-water contact angle is only 33°. After modification, the contact angle of SMs gradually increased from 54 ° to 121° (Figure 2a) depending on the amount of *n*-octyltrimethoxysilane used (EDS mapping and FTIR spectrum of octyl-modified SMs are provided in Supplementary Figure 7). When the air-water contact angle was less than 70°, the droplets immediately broke up upon contact with SMs (Figure 2a). In cases where the contact angle is in the range of 70°–100°, the droplets began to coexist with SMs in the continuous-flow system although the uniform spherical morphology deformed to some extent. However, when the contact angle is above 100°, a stable co-packed system was established and the morphology of droplets was well maintained in the mixed system. These results show that SMs possessing hydrophilic surfaces tend to disturb the interface of PEDs, whereas more hydrophobic SMs do not (compared to the aforementioned neat Pickering emulsion system). This phenomenon can be explained in terms of the interfacial energies *E* of the mixed system (Figure 2b and Supplementary Figure 8). In the case of the IL drop partially engulfing a SM, the surface area of the IL-oil interface S_1 within PEDs, the contact area S_2 between PEDs and SMs and the contact area S_3 between oil and SMs can be written as follows[42]:

$$S_1 = 2\pi R^2(1 - \cos\alpha_2) \quad (1)$$

$$S_2 = 2\pi r^2(1 - \cos\alpha_1) \quad (2)$$

$$S_3 = 2\pi r^2(1 + \cos\alpha_1) \quad (3)$$

where *R* is the droplet radius in PEDs, *r* is the radius of SMs and α_1 and α_2 are the central angles. The total interfacial energy *E* can be written as:

$$E = S_1\gamma_{IL-o} + S_2\gamma_{IL-SMs} + S_3\gamma_{SMs-o} \quad (4)$$

where $\gamma_{IL\text{-}o}$, $\gamma_{IL\text{-}SMs}$ and $\gamma_{SMs\text{-}o}$ denote the interfacial tensions at the IL-oil, IL-SMs and SMs-oil interfaces, respectively. In order to facilitate calculation, we do not take into account the impact of the movement of SMs on the curvature of PEDs. I don't understand this-explain Thus, $R = r$ and $\alpha_2 = \pi\text{-}\alpha_1$. Substituting equations (1-3) into (4), we obtain

$$E = 4\pi R^2\gamma_{IL-SMs} \quad (5)$$

I could not obtain eq.(5) from (1)-(4)??

Obviously, the decrease in the water contact angle of SMs will also lead to a decrease in the interfacial tension γ_{IS} this is not necessarily true as contact angle is determined by the balance of 3 interfacial tensions . Therefore, lower interfacial energies are gained when the interface of PEDs is occupied by SMs. Consequently, hydrophilic SMs tend to migrate into the IL phase and are reluctant to reside at the IL-oil interface or in the oil phase, inducing droplet disruption. The explanation is in good agreement with our experimental observations (Supplementary Figures 8 and 9). As the hydrophobicity of SMs increases, they begin to migrate to the IL−oil interface and then reside at the interfaces of the droplets and finally SMs prefer to disperse in the oil phase. this is true in the absence of silica nanoparticles but not in their presence (as they are already in oil in the first place)

I am not clear what this paragraph is meant to be showing: there are some incorrect statements also.

The role played by SMs in the co-packed system was further confirmed by the dependence of the stability of the co-packed system on the volume fraction of SMs. To accelerate the evaluation, the co-packed systems were heated to 120 °C. The Pickering emulsion in the absence of SMs was completely demulsified after 20 h (Figure 2c and Supplementary Figure 10). However, when the volume fraction of SMs was 30%, the co-packed system became stable without noticeable droplet

coalescence (Figure 2c). This is also true for the case where the volume fraction was raised up to 50% and 67%. Comparison of the corresponding size distributions of droplets before and after the thermal treatment reveals that with an increase in the volume fraction of SMs, the change in droplet size became less pronounced after thermal treatment (Figure 2d). An "isolation" mechanism is proposed here to explain this phenomenon. The fusion of droplets with their neighbors is the main reason for demulsification, which is accelerated at high temperature[40]. When these droplets are isolated or surrounded by neighboring SMs, three-dimensional rigid networks were formed. This physical obstruction enables the droplets to be spatially separated thereby reducing the possibility of them being in contact (Figure 2e)[40]. At the same time, the three-dimensional rigid network with SMs as rigid pillars can withstand the applied pressure coming from the mobile phase still unclear-explain which accounts for the aforementioned observation that the co-packed system is more mechanically robust than the neat Pickering emulsion droplet-packed system. The sufficient robustness is crucial for the establishment of continuous-flow reaction systems.

Continuous-flow cascade reaction. (*S*, *S*)-{(salen)Ti-(μ-O)}$_2$ (Ti(Salen), molecular complex) and *Candida Antarctica lipase* B (CALB) were chosen as two representative catalysts for the cascade synthesis of chiral *O*-acylated cyanohydrin, an important pesticide and drug intermediate[43-45]. As Figure 3a shows, Ti(Salen) is used to catalyze the first step in this cascade reaction, namely asymmetric addition of acetyl cyanide to aldehydes yielding chiral *O*-acylated cyanohydrins. Ti(Salen) has good catalytic activity but offers a relatively low enantioselectivity towards the targeted enantiomer[44,45]. It was reported that addition of CALB into the Ti(Salen)-containing system could improve the enantioselectivity through hydrolyzing a unwanted enantiomer of *O*-acylated

cyanohydrin back to the starting reactant[43]. After multiple cycles, the starting reactants could be completely converted to the desired enantiomer. This ideal cascade design, however, was experimentally discounted due to the incompatibility between Ti(Salen) and CALB[46]. This incompatibility led to a requirement of stepwise addition of CALB and taking as long as 144 h to obtain a satisfactory enantioselectivity.

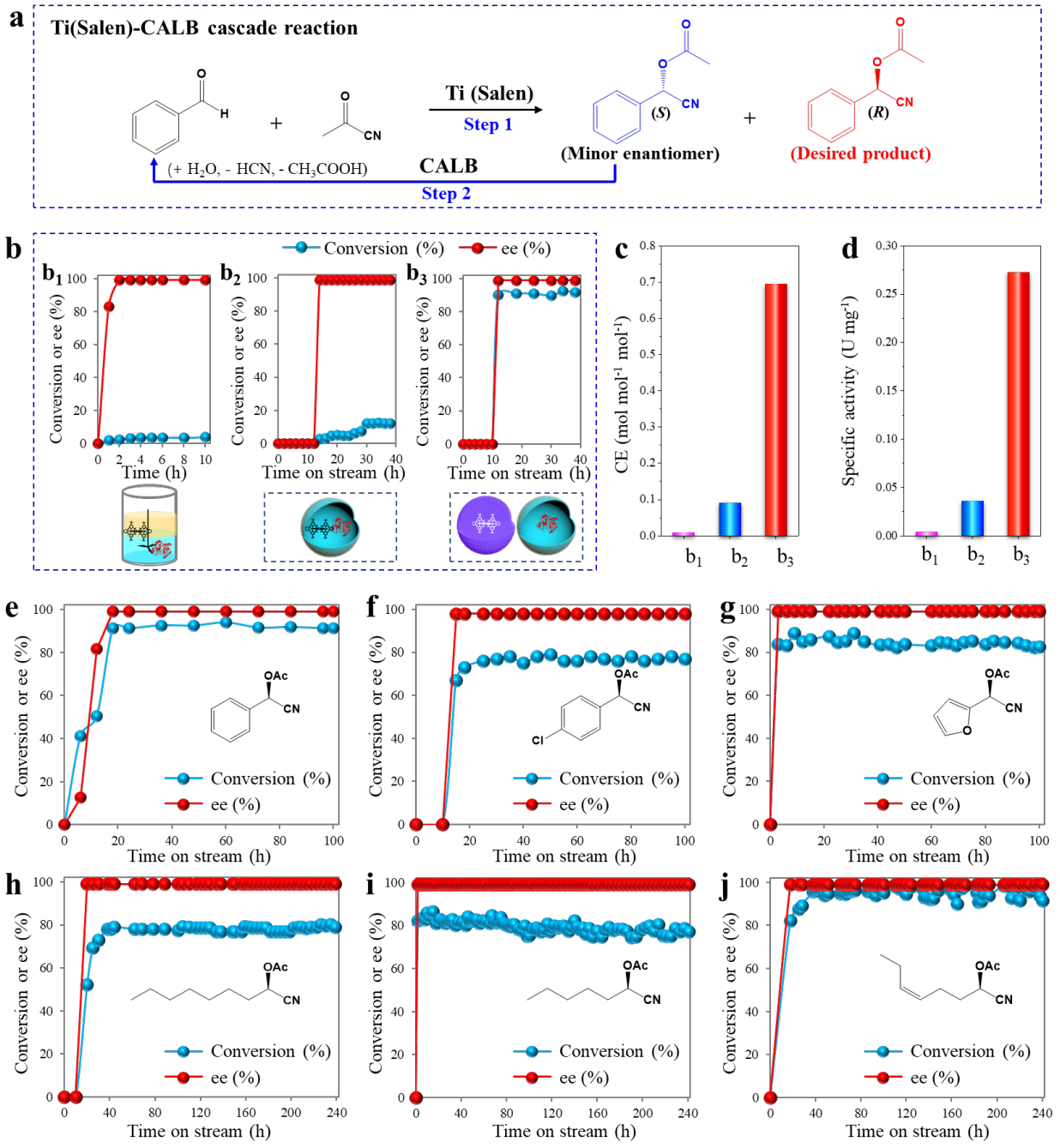

Fig. 3 | Chemo-enzymatic cascade synthesis of cyanohydrin. a Cascade reaction using Ti(Salen)

and CALB as catalysts. **b** Conversion and e.e. with time in batch and flow systems. **b_1** Batch reaction using Ti(Salen) and CALB as catalysts. Reaction condition: 1.4 mL [BMIM]PF_6, 2 mL PEG-300 (assists in dissolution of water in IL which is a reactant), 0.6 mL PBS (pH = 7.4, 0.05 M), 0.2 mL CALB (8.0 mg ml^{-1} of protein), 80 mg Ti(Salen), 30 mg 4-dimethylaminopyridine (DMAP, as co-catalyst), 2 mL *n*-octane containing benzaldehyde (0.05M) and acetyl cyanide (0.2M), 25 ℃, 900 rpm. **b_2** Flow reaction in the Ti(Salen)-CALB@PEDs packed system. Ti(Salen)-CALB@PEDs consist of 1.4 mL [BMIM]PF_6, 2 mL PEG-300, 0.6 mL PBS (pH = 7.4, 0.05 M), 0.2 mL CALB, 80 mg Ti(Salen), 30 mg DMAP, 2 mL *n*-octane, 0.2 g emulsifier. **b_3** Flow reaction in the CALB@PEDs and Ti(Salen)/SMs co-packed system. CALB@PEDs consist of 0.7 mL [BMIM]PF_6, 1 mL PEG-300, 0.3 mL PBS (pH = 7.4, 0.05 M), 0.2 mL CALB, 1 mL *n*-octane, 0.1 g emulsifier then mixed with 0.3 g Ti(Salen)/SMs (containing 80 mg Ti(Salen) and 30 mg DMAP). Flow reaction conditions: Benzaldehyde (0.05 M) and acetyl cyanide (0.2 M) in *n*-octane as mobile phase, 25 ℃, flow rate = 1 mL h^{-1}. **c** Catalysis efficiency in the batch and flow reactions. **d** Specific activity of CALB in different systems. For batch reaction, CE and specific activity were calculated according to the conversion within the first 6 h; for the flow reactions, CE was calculated after the conversion leveled off. **e, f** Different substrates for Ti(Salen)-CALB cascade flow reactions. Reaction conditions: Dosages of CALB@PEDs and Ti(Salen)/SMs in **e**, **g** and **h** are the same as **b_1** but are twice as high in **f**, **i** and **j**. Aldehyde (0.05 M) and acetyl cyanide (0.2 M) in *n*-octane as mobile phase, 25 °C. Flow rate: **e** 1 to 0.8 mL h^{-1}, **f** 1.0 to 0.5 mL h^{-1}, **g** 1.0 to 0.5 mL h^{-1}, **h** 0.8 to 0.3 mL h^{-1}, **i** 0.8 to 0.3 mL h^{-1}, **j** 0.5 to 0.2 mL h^{-1}.

still too many graphs in this figure

Ti(Salen) was supported on the pore walls of SMs with a aid of strong interactions between titanium in Ti(Salen) and silanol groups on the surface of SMs[26,47], generating a solid microsphere catalyst Ti(Salen)/SMs (400 mg g^{-1} of Ti(Salen)). CALB was dissolved within the IL-based PEDs, yielding CALB-containing droplets named as CALB@PEDs (0.73 mg mL^{-1} of protein). Homogenous distribution of Ti(Salen) or CALB throughout the whole body of the SMs or PEDs was achieved, evidenced by the presence of homogeneous green fluorescent (from the intrinsic fluorescence of Ti(Salen)) or red fluorescent signals (from RBITC labeled CALB) respectively (Supplementary Figures 11a and b). The co-packed system with Ti(Salen)/SMs and CALB@PEDs exhibited good ability to confine CALB or immobilize Ti(Salen) since there is no catalyst crosstalk between SMs and PEDs after mixing and even after standing for 48 h, confirmed by fluorescent observations (Supplementary Figures 11c and 12).

Before examining the continuous-flow system, we carried out a set of batch and continuous-flow reactions for comparison. For the batch reactions, a traditional biphasic reaction in the presence of both Ti(Salen) and CALB was examined. After 10 h, the benzaldehyde conversion was only 3.7% (Figure 3b$_1$), although 99% e.e. of O-acylated cyanohydrin was obtained. This batch reaction was translated to a continuous-flow reaction, *i.e*. Pickering emulsion droplet-packed system, in which Ti(Salen) and CALB were co-confined within the same droplet how was this achieved? this needs stating clearly. An 8.5% conversion was achieved after steady-state was established (Figure 3b$_2$). The low cascade efficiency was caused by the intrinsic incompatibility of Ti(Salen) and CALB[26,46]. Encouragingly, in our co-packed continuous-flow system, the benzaldehyde conversion at steady-state was increased up to 81% and the e.e. for *O*-acylated cyanohydrin was 99% (Figure 3b$_3$). According to these results, we estimated the catalytic efficiency CE (defined as moles of converted reactant per mole of Ti per h, *i.e*. mol mol^{-1} h^{-1}, Figure 3c) based on Ti and the activity of CALB (expressed as μmol of substrate converted per min per mg enzyme, *i.e*. U mg^{-1}, Figure 3d), respectively. The co-packed system gave a CE of 0.69 mol mol^{-1} h^{-1}. This value is about 7.6 times higher than that of Ti(Salen) and CALB co-confined in the same droplets in the flow system (b$_2$: 0.09 mol mol^{-1} h^{-1}) and 76.8 times higher than that of the direct mixing of Ti(Salen) and CALB in the conventional biphasic batch system (b$_1$: 0.009 mol mol^{-1} h^{-1}). Meanwhile, the activity of CALB in the co-packed continuous-flow system was 0.27 U mg^{-1}, exhibiting 7.5 and 67.8-fold enhancement relative to system b$_2$ and b$_1$ respectively (Figure 3d). These results emphasize the significant benefits of our co-packed system.

Next, we checked various aldehydes including benzaldehyde, 4-chlorobenzaldehyde, furfuraldehyde, octanaldehyde, hexaldehyde and *cis*-4-heptenal (Figure 3e-j). For all of the

investigated substrates, the substrate conversions increased to more than 75% and then leveled off after reaching steady-state. For benzaldehyde, 4-chlorobenzaldehyde and furfuraldehyde (Figure 3e-g), as high as 77-92% conversions were obtained and their e.e. of chiral product was always larger than 99%. After continuous operation lasting up to 100 h, no significant decrease in their overall conversions or e.e. was observed. For long-chain aldehydes such as octanaldehyde, hexaldehyde and cis-4-heptenal, we prolonged the running time to 240 h; the e.e. of chiral products were still > 99% and the conversions were always maintained between 79% and 95% (Figure 3h-j). The SMs and PEDs were still well preserved in terms of both their size and morphology after 240 h of continuous-flow reaction (Supplementary Figure 13). Inductively coupled plasma-mass spectrometry (ICP-MS) showed that *ca*. 95% of Ti was retained in the fixed-bed reactor after 48 h of flow reaction, while the retention of CALB was determined to be greater than 99% (Supplementary methods 4). Such a high stability may be ascribed to the confinement effects of the IL-based PEDs and SMs towards the metal complex and enzyme, respectively.

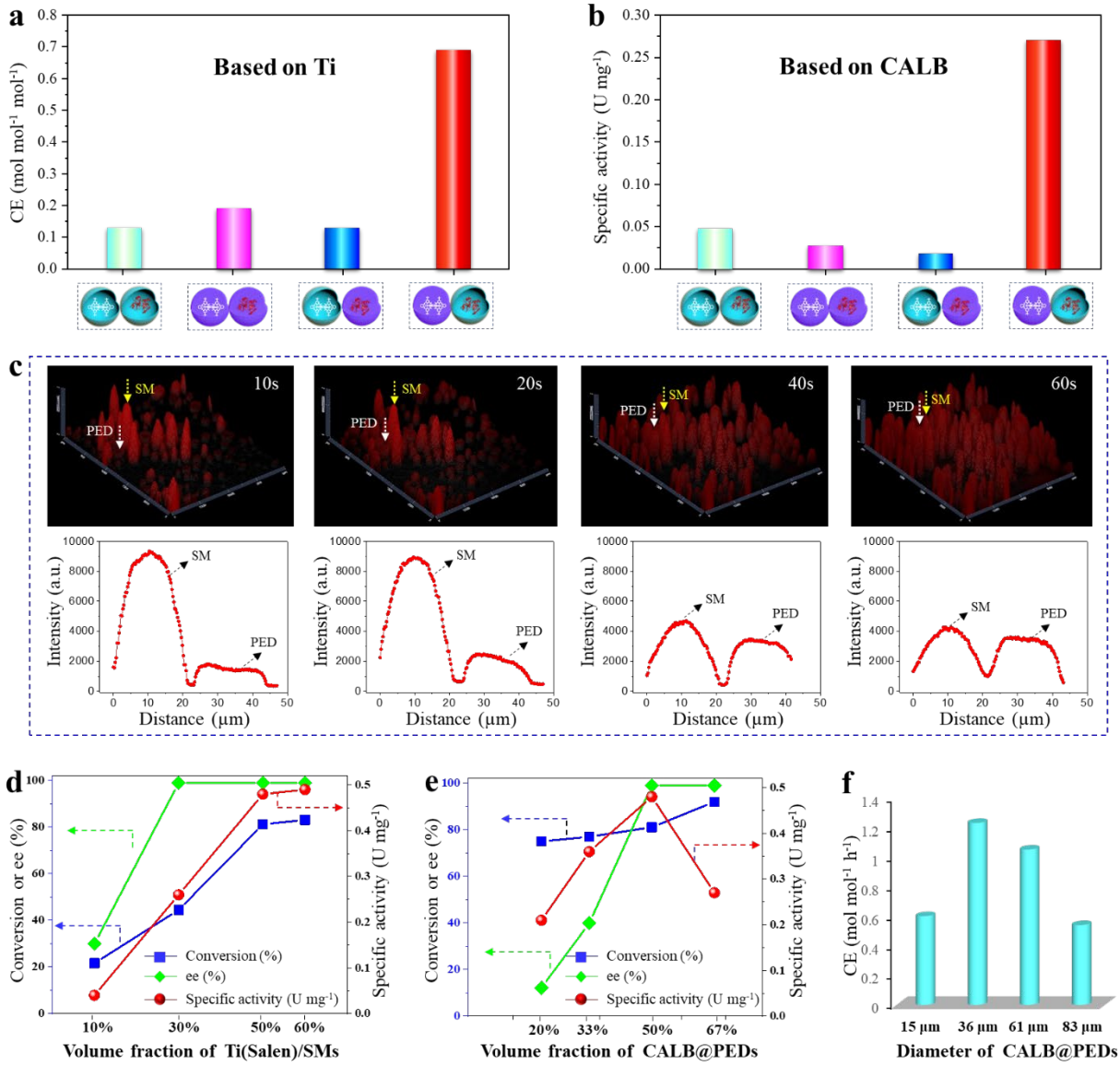

Fig. 4 | Directional transport effect. a Catalysis efficiency in different flow systems. **b** Specific activity of CALB in different flow systems. **c** Fluorescence microscopy images with time for the transfer of 5 μM rhodamine B from SMs to PEDs and the curves showing the variation in fluorescence intensity. x-axis and y-axis display the spatial distance and fluorescence intensity respectively. **d** Benzaldehyde conversion, e.e. and specific activity as a function of the volume fraction of Ti(Salen)/SMs. **e** Conversion, e.e. and specific activity as a function of the volume fraction of CALB/PEDs. **f** CE for the different droplet diameters with fixed size of SMs. All reaction conditions are the same as those in Figure 3b$_3$ except for the catalyst ratios and flow rate (2 mL h^{-1} here).

Directional reaction intermediate transportation from SMs to PEDs. The superior cascade efficiency encouraged us to investigate the working principles underlying our co-packed system. To this end, a set of co-packed systems were constructed by varying the location of Ti(Salen) and CALB in/on PEDs or SMs, including four cascade pairs: Ti(Salen)/PEDs + CALB@PEDs (Ti(Salen) and CALB are both dissolved or dispersed within the different droplets), Ti(Salen)/SMs + CALB/SMs (Ti(Salen) and CALB are both supported on different SMs), Ti(Salen)/PEDs + CALB/SMs and Ti(Salen)/SMs + CALB@PEDs. The Ti(Salen)/PED + CALB@PED co-packed system after steady-state offered a benzaldehyde conversion of 17.8 in 98% e.e. (Supplementary Figure 14a). The benzaldehyde conversion was seen to increase up to 41% for the Ti(Salen)/SMs + CALB/SMs co-packed system but the e.e. was only 21.5% (Supplementary Figure 14b). The Ti(Salen)@PED + CALB/SM co-packed system offered a conversion of 24.2% and an e.e. of 24.3% (Supplementary Figure 14c). Remarkably, the Ti(Salen)/SM + CALB@PED co-packed system offered an 81% conversion and an e.e. of 99% (Figue 3b$_3$). On the basis of the conversions and e.e., the CEs for these four systems in terms of Ti were calculated to be 0.13, 0.19, 0.12 and 0.69 mol mol^{-1} h^{-1} (Figure 4a). Meanwhile, the specific activity of CALB was estimated to be 0.05, 0.03, 0.02 and 0.27 U mg^{-1} (Figure 4b). Apparently, despite fixing the Ti(Salen) or CALB dosages in these systems, the catalytic efficiency obtained in the Ti(Salen)/SM and CALB@PED co-packed system is outstanding among these four systems.

In view of the substantial difference in the catalytic efficiency, we speculate that there exists a directional reaction intermediate transfer from SMs to PEDs in our co-packed system. To validate this hypothesis, the fluorescent probe reagent rhodamine B was used to track molecular transport between SMs and PEDs. Prior to this tracking, we tested the permeability of these two individual

microreactors, SMs and PEDs, which is a pre-requisite for molecular transfer between them. As Supplementary Figure 15 displays, once IL-based PEDs in oil were brought into contact with an ethanolic solution of rhodamine B, the fluorescent molecules quickly diffused into the interior of PEDs within 10 s and the fluorescence intensity in the center was observed to gradually level off after 20 s. This observation indicates that the IL-based PEDs are highly permeable towards exterior molecules. Similar to IL-based PEDs, SMs also exhibited a good permeability (Supplementary Figure 16). After confirming the good permeability of the two individual microreactors, rhodamine B was initially loaded onto SMs with which PEDs in oil were then brought into contact. Interestingly, the red fluorescent probe molecules passed through the oil phase between SMs and PEDs and rapidly diffused into droplets within 10 s, mirrored by the presence of a red fluorescent pattern within the droplets (Figure 4c). The fluorescence intensity in the center of SMs was observed to gradually decrease as it increased within the interior of the PEDs with time (Figure 4c). After 60 s, the fluorescence intensity for the droplet was equal to that for the SMs. In contrast, the rate of molecular transport from PEDs to SMs was relatively slow. About 100 s was taken to reach fluorescence intensity levelling off (twice as long for SMs to PEDs; Supplementary Figure 17a). Notably, more than 120 s was taken for the transport of fluorescent molecules from PEDs to PEDs while almost no transport occurred for the SMs-SMs system (Supplementary Figures 17b and c). These results strongly suggest that the fluorescent molecules can transport between SMs and PEDs, and the transport rate was the fastest in the case of molecular transport from SMs to PEDs. This is because the ionic liquid has a capability to enrich organics from the surroundings with a lower affinity to organic molecules[38]. Such a directional molecular transport is in part responsible for the high catalysis efficiency of our co-packed system.

The above interesting results prompt us to investigate the impact of the ratio of SMs to PEDs and their sizes on the cascade reaction. Two sets of co-packed systems with different volume ratios of SMs to PEDs were examined (their sizes are equal, see Supplementary Figure 18). It was found that the conversions, e.e. and even the specific activity of enzyme were dependent on the ratio. In the first set of experiments, the volume fraction of Ti(Salen)/SMs was varied from 10 to 30, 50 and 60% (with respect to total volume of the co-packed system; the local concentration of Ti(Salen) was fixed) while keeping the amount of CALB@PEDs constant. The benzaldehyde conversion at steady-state increased from 21.6 to 44.5, 81.2 and 83.1% (Figure 4d and Supplementary Figure 19), which is understandable in that the amount of Ti(Salen) increases. However, the e.e. of the product increased from 29.9 to 99, 99 and 99% and the corresponding activity of the enzyme was also changed from 0.04 to 0.26, 0.48 and 0.49 U mg^{-1} although its amount was kept constant. The increased local intermediate concentration arising from more Ti(Salen) available is beneficial in accelerating the second step of the reaction. Similarly, in the second set of experiments, the volume fraction of CALB@PEDs was varied from 20 to 33, 50 and 67% (the local concentration of enzyme was fixed) while keeping the amount of Ti(Salen)/SMs constant. The e.e. of the product increased from 12.2 to 39.9, 99 and 99% (Figure 4e and Supplementary Figure 20) despite the fact that the enzyme activity first increased and then decreased. Interestingly again, the benzaldehyde conversion at steady-state also increased from 75 to 77, 81.1 and 92% although the amount of Ti(Salen) was not altered this time. It is likely that more enzyme in the system accelerates the consumption of the intermediate, shifting the equilibrium of the first step of the cascade reaction. These findings point out the fact that the fraction of SMs or PEDs significantly affects the kinetics of each step of the cascade reaction besides the overall reaction, even though one of them is not varied in the dosage. This synergism is

realized though timely transfer of the intermediate from SMs to PEDs.

At the same time, the sizes of PEDs and SMs were found to impact the catalytic efficiency. As Figure 4f shows, PEDs with different diameters were co-packed with SMs of correspondingly similar sizes (15, 36, 61, 83 μm in diameter; Supplementary Figure 21) while the amounts of Ti(Salen) and CALB were both fixed. It is interesting to find that when the droplet diameter increased, both the benzaldehyde conversion and the e.e. of the product at steady-state first increased and then decreased (Supplementary Figure 22). The corresponding CE was calculated to be 0.6, 1.23, 1.05 and 0.54 mol mol^{-1} h^{-1}, displaying a maximum for droplets of 36 μm in diameter (Figure 4f). The size-dependent effect can be attributed to the correlation between the microreactor size and the utilization efficiency of catalysts[25,26]. When the microreactors are too big, the amount of catalyst within the droplets is in excess and a portion of them are idle leading to a low catalytic efficiency. On the contrary, if the microreactor is too small, the amount of catalyst within the individual microreactors is insufficient and the reaction is accordingly incomplete. The reactant or intermediate molecules need to travel to the neighboring microreactor to locate catalysts. The additional diffusion pathway results in lowering of the catalytic efficiency. These results illustrate that our co-packed system is customizable to some extent through alternation of the numbers and sizes of PED and SM microreactors, thereby providing a potential bottom-up approach to control macroscopic cascade reactions.

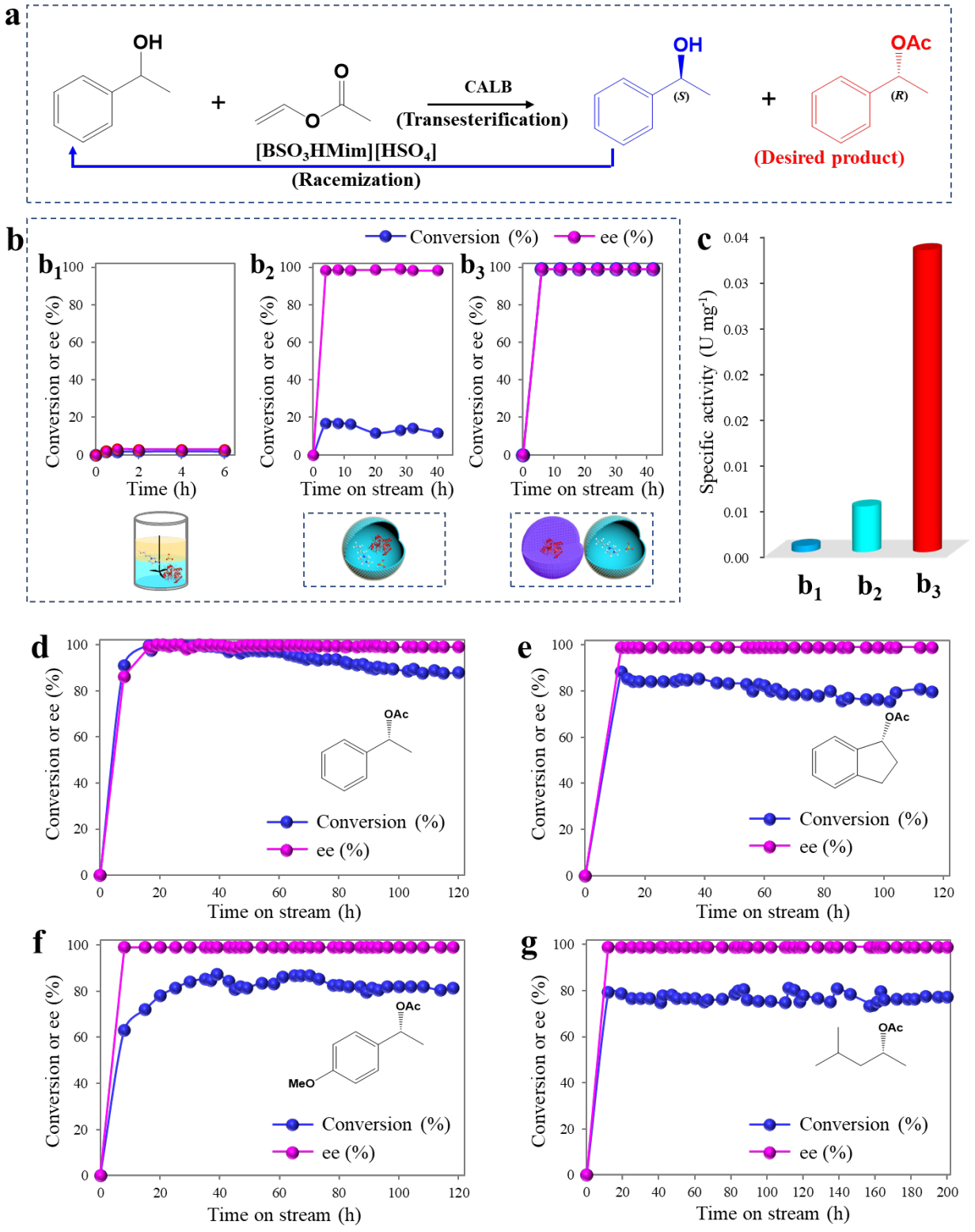

Fig. 5 | Cascade catalytic synthesis of chiral esters using $[BSO_3HMim]HSO_4$ and CALB as catalysts. **a** Cascade reaction. **b** Conversion and e.e. with time in batch and flow systems. **b_1** Batch reaction using $[BSO_3HMim]HSO_4$ and CALB as catalysts. Reaction condition: 4 mL $[BMIM]BF_4$, 0.025 g $[BHSO_3MIM]HSO_4$, 0.03 mL CALB (8.0 mg mL^{-1} of protein), 2 mL *n*-octane containing 1-phenylethanol (0.05 M) and vinyl acetate (0.2 M), 45 °C, 600 rpm. **b_2** Flow reaction in

[BSO_3HMim]HSO_4-CALB@PEDs packed system. The [BSO_3HMim]HSO_4-CALB@PEDs consists of 4 mL [BMim]BF_4, 0.025 g [BSO_3HMim]HSO_4, 0.03 mL CALB, 2 mL *n*-octane and 0.12 g silica emulsifier. **b_3** Flow reaction in the [BSO_3HMim]HSO_4@PEDs and CALB/SMs co-packed system. The [BSO_3HMim]HSO_4@PEDs consists of 2 mL [BMim]BF_4, 0.025 g [BSO_3HMim]HSO_4, 0.03 mL CALB, 1 mL *n*-octane and 0.06 g silica emulsifier then mixed with 0.3 g CALB/SMs (54 mg g^{-1} of protein). Flow reaction conditions: Alcohol (0.05 M) and vinyl acetate (0.2 M) in *n*-octane as mobile phase, 45 °C, flow rate = 1 mL h^{-1}. **c** Specific activity of CALB in batch and flow systems. The specific activity of CALB was calculated according to the conversion within the first 2 h for the batch reactions and after the conversion leveled off for the flow reactions. **d-g** Substrate scope extension. Reaction conditions: The dosages of [BSO_3HMim]HSO_4@PEDs and Ti(Salen)/SMs in **d** and **g** are the same as **b_3**, while they are twice in **e** and **f**. Alcohol (0.05 M) and vinyl acetate (0.2 M) in *n*-octane as mobile phase, 45 °C. Flow rate: **d** 1 to 0.5 mL h^{-1}, **e** 0.8 to 0.6 mL h^{-1}, **f** 0.8 to 0.4 mL h^{-1}, **g** 0.8 to 0.5 mL h^{-1}.

Cascade reaction extension. We further applied the co-packed protocol to another chemo-enzymatic cascade reaction consisting of two steps: CALB-promoted dynamic kinetic resolution of racemic 1-phenylethanol and acid-catalyzed racemization of 1-phenylethanol (an IL [BSO_3HMim]HSO_4 was used as catalyst) does it dissolve in the main IL? not answered! in sequence (Figure 5a)[48-50]. The main challenge for this cascade reaction is the incompatibility between acid catalyst and enzyme[48]. For instance, in a batch reaction where [BSO_3HMim]HSO_4 and CALB were directly mixed in water? not answered!, the conversion of 1-phenylethanol was only 2% after 6 h (Figure 5b_1). When this batch system was translated to the continuous-flow system where the [BSO_3HMim]HSO_4 and CALB were dissolved within the same Pickering emulsion droplets, still only 14.5% conversion was obtained after reaching a steady-state (Figure 5b_2). Interestingly, when utilizing the co-packed system with [BSO_3HMim]HSO_4@PEDs and CALB/SMs, the conversion of 1-phenylethanol at steady-state rapidly rose up to 99% and the e.e. of the ester was as high as 99% (Figure 5b_3). The specific activity of CALB in the latter was calculated to be 0.033 U mg^{-1}, which is 6.7 times higher than that for the co-localization of [BSO_3HMim]HSO_4 and CALB within the same droplet in the continuous-flow system and 47.1 times higher than that of direct mixing of

[BSO_3HMim]HSO_4 and CALB (Figure 5c) in batch. Notably, after further prolonging the running time to 120 h, *ca*. 88–99% conversion of 1-phenylethanol and 99% e.e. of the chiral ester was still maintained (Figure 5d). In comparison to the reported systems, our co-packed system works more efficiently in terms of enzyme (2.5 times) in addition to the simple work-up[48,49]. Moreover, for other racemic compounds such as 1-indanol, 1-(4-methoxyphenyl)ethanol and 4-methyl-2-pentanol, 75-88% conversions and > 99% of e.e. of chiral esters were obtained over 120-200 h (Figure 5e-g). These results further confirm the broad applicability of our co-packed system.

Conclusions

In conclusion, we have successfully developed a conceptually novel continuous-flow cascade catalytic system based on co-packing of Pickering emulsion droplets and solid microspheres. We find that the stability of Pickering emulsion droplets is enhanced by the presence of sold microspheres under flow and pressured conditions. The underpinning principle is found to be the surface interactions between solid microspheres and emulsion droplets, which is governed by the wettability of the former. In two independent chemo-enzymatic cascade reactions involving the catalysts Ti(Salen)+CALB and acid+CALB, the droplet and solid microsphere co-packed system was shown to work very efficiently for continuous-flow synthesis of chiral O-acylated cyanohydrins and chiral 1-phenylethanol acetate, highlighted by maintaining 99% e.e. over 100–240 h. Impressively, the reaction efficiency of the co-packed continuous-flow system was improved between 7 and 77-fold relative to the batch and flow systems. Moreover, the overall cascade efficiency can be easily tuned by altering both the number ratio of Pickering emulsion droplets to solid microspheres as well as the droplet size. Impressively, crucial to the high CE may be the directional transport of reaction intermediates from SM to PED microreactors, which is unattainable

in the existing systems. Being operationally simple and adaptable, our co-packed system provides an unprecedented platform for cascade reactions involving homogeneous catalysts, heterogeneous catalysts and enzymes.

Methods

preparation of Pickering emulsion is not here or in Supp. Info.

it must include why PEG-300 is added!

General procedures for the preparation of droplet and solid microsphere co-packed reaction systems. A given volume of IL-in-oil Pickering emulsion was uniformly mixed with a given volume of solid microspheres of comparable size. The obtained mixture was then gently filled into a glass column reactor as the fixed phase, thus forming a droplet and solid microsphere co-packed continuous-flow system. The inner diameter of the column was 2 cm and it was equipped with a sand filter (pore diameter 4.5–9 μm) and a valve at the bottom. If needed, the column was wrapped with a thermo-jacket for heating. The continuous oil phase was continuously pumped into the column from the top, and the downstream was collected from the outlet of the column. The flow rate was tuned through a piston pump (LC-01P, Jiangshen Technology Co., China) and also determined based on the volume of the collected liquid per unit time.

Chemo-enzymatic cascade synthesis of chiral O-acylated cyanohydrins in PED and SM co-packed bed reactors. A mixture of 0.7 mL [BMIM]PF_6, 1.0 mL PEG-300, 0.3 mL H_2O, 0.01 g Na_2HPO_4, 0.2 mL CALB, 4 mL of *n*-octane and 0.066 g silica emulsifier was stirred at 8000 rpm for 2 min, generating an IL-in-oil Pickering emulsion. This obtained Pickering emulsion was mixed with

0.3 g Ti(Salen)/SMs. The resultant mixture was gently loaded into a glass column reactor (inner diameter of 2 cm) with a sand filter (pore diameter 4.5−9 μm) placed at the bottom of the column. A solution of aldehydes (0.05 M) and acetyl cyanide (0.2 M) in *n*-octane as mobile phase was pumped at a given flow rate and was allowed to pass through the column reactor whose temperature was kept at 25 °C. The outflow of the column reactor was sampled for GC analysis (equipped with a chiral column) at regular intervals and the product was further confirmed with GC–MS.

References

1 Schrittwieser, J. H., Velikogne, S., Hall, M. & Kroutil, W. Artificial biocatalytic linear cascades for preparation of organic molecules. *Chem. Rev*. 118, 270–348 (2018).

2 Vázquez-González, M., Wang, C. & Willner, I. Biocatalytic cascades operating on macromolecular scaffolds and in confined environments. *Nat. Catal*. 3, 256–273 (2020).

3 Sperl, J. M. & Sieber, V. Multienzyme cascade reactions—status and recent advances. *ACS Catal.* **8**, 2385−2396 (2018).

4 Schrittwieser, J. H., Velikogne, S., Hall, M. & Kroutil, W. Artificial biocatalytic linear cascades for preparation of organic molecules. *Chem. Rev*. **118**, 270−348 (2018).

5 Rudroff, F. et al. Opportunities and challenges for combining chemo- and biocatalysis. *Nat. Catal.* **1**, 12−22 (2018).

6 Britton, J. & Raston, C. L. Multi-step continuous-flow synthesis. *Chem. Soc. Rev*. **46**, 1250−1271 (2017).

7 Jiao, J. et al. Multi-step continuous-flow organic synthesis: opportunities and challenges. *Chem. Eur. J*. **27**, 4817−4838 (2021).

8 Contente, M. L. & Paradisi, F. Self-sustaining closed-loop multienzyme mediated conversion of amines into alcohols in continuous reactions. *Nat. Catal*. 1, 452–459 (2018).

9 Tsubogo, T., Oyamada, H. & Kobayashi, S. Multistep continuous-flow synthesis of (R)- and (S)-rolipram using heterogeneous catalysts. *Nature* **520**, 329−332 (2015).

10 Sagmeister, P. et al. Advanced real-time process analytics for multistep synthesis in continuous-flow. *Angew. Chem. Int. Ed*. **60**, 8139−8148 (2021).

11 Wang, H. et al. Biomimetic enzyme cascade reaction system in microfluidic electrospray microcapsules. *Sci. Adv*. **4**, eaat2816 (2018).

12 Russell, M. G. & Jamison, T. F. Seven-step continuous-flow synthesis of linezolid without intermediate purification. *Angew. Chem. Int. Ed*. **58**, 7678−7681 (2019).

13 Borah, P., Fianchini, M. & Pericàs, M. A. Assessing the role of site isolation and compartmentalization in packed-bed flow reactors for processes involving wolf-and-lamb scenarios. ACS Catal. **11**, 6234−6242 (2021).

14 Wang, M. et al. Combining Pd nanoparticles on MOFs with cross-linked enzyme aggregates of lipase as powerful chemoenzymatic platform for one-pot dynamic kinetic resolution of amines. *J. Catal.* **378**, 153–163 (2019).

15 Saito, Y., Nishizawa, K., Laroche, B., Ishitani, H. & Kobayashi, S. Continuous-flow synthesis of (R)-tamsulosin utilizing sequential heterogeneous catalysis. *Angew. Chem. Int. Ed*. **61**, e202115643 (2022).

16 Li, Z. L. et al. Highly selective conversion of carbon dioxide to aromatics over tandem catalysts. *Joule* **3**, 570–583 (2019).

17 Ichitsuka, T., Takahashi, I., Koumura, N., Sato, K. & Kobayashi, S. Continuous synthesis of aryl amines from phenols utilizing integrated packed-bed flow systems. *Angew. Chem. Int. Ed*. **59**, 15891−15896 (2020).

18 Durndell, L. J. et al. Cascade aerobic selective oxidation over contiguous dual-catalyst beds in continuous-flow. *ACS Catal*. **9**, 5345−5352 (2019).

19 Mattey, A. P. et al. Development of continuous-flow systems to access secondary amines through previously incompatible biocatalytic cascades. *Angew. Chem. Int. Ed.* **60**, 18660−18665 (2021).

20 Wheeldon, I. et al. Substrate channelling as an approach to cascade reactions. *Nat. Chem*. **8**, 299−309 (2016).

21 Isaacs, M. A. et al. A spatially orthogonal hierarchically porous acid–base catalyst for cascade and antagonistic reactions. *Nat. Catal*. **3**, 921−931 (2020).

22 Vázquez-González, M., Wang, C. & Willner, I. Biocatalytic cascades operating on macromolecular scaffolds and in confined environments. *Nat. Catal*. 3, 256−273 (2020).

23 Rabe, K. S., Muller, J., Skoupi, M. & Niemeyer, C. M. Cascades in compartments: en route to

machine-assisted biotechnology. *Angew. Chem. Int. Ed*. **56**, 13574−13589 (2017).

24 Zhang, M. et al. Compartmentalized droplets for continuous-flow liquid-liquid interface catalysis. *J. Am. Chem. Soc*. **138**, 10173−10183 (2016).

25 Zhang, M. et al. Ionic liquid droplet microreactor for catalysis reactions not at equilibrium. *J. Am. Chem. Soc*. **139**, 17387−17396 (2017).

26 Zhang, M. et al. Pickering emulsion droplet-based biomimetic microreactors for continuous-flow cascade reactions. *Nat. Commun*. **13**, 475 (2022).

27 Zhao, H., Ran, R., Wang, L., Li, C. S. & Zhang S. J. Novel continuous process for methacrolein production in numerous droplet reactors. *AIChE J*. **66**, e16239 (2020).

28 Zhang, H., Shang M. j., Zhao, Y. C. & Su, T. H. Process intensification of 2,2'-(4-nitrophenyl) dipyrromethane synthesis with a SO_3H-functionalized ionic liquid catalyst in Pickering-emulsion-based packed-bed microreactors. *Micromachines* **12**, 796 (2021).

29 Wu, H., Du, X., Meng, X., Qiu, D. & Qiao, Y. A three-tiered colloidosomal microreactor for continuous-flow catalysis. *Nat. Commun.* **12**, 6113 (2021).

30 Tang, X. P. et al. Heteropoly acids-functionalized Janus particles as catalytic emulsifier for heterogeneous acylation in flow ionic liquid-in-oil Pickering emulsion. *Colloid Surface A* **570**, 191–198 (2019).

31 Crossley, S., Faria, J., Shen, M. & Resasco, D. E. Solid nanoparticles that catalyze biofuel upgrade reactions at the water/oil interface. *Science* **327**, 68–72 (2010).

32 Wei, Q. B. et al. Recognition of water-induced effects toward enhanced interaction between catalyst and reactant in alcohol oxidation. *J. Am. Chem. Soc.* **143**, 16, 6071–6078 (2021).

33 Pera-Titus, M., Leclercq, L., Clacens,J. M., De Campo, F. & Nardello-Rataj, V. Pickering interfacial catalysis for biphasic systems: from emulsion design to green reactions. *Angew. Chem. Int. Ed*. **54**, 2006–2021 (2015).

34 Sun, Z., Glebe, U., Charan, H., Bçker, A. & Wu, C. Z. Enzyme–polymer conjugates as robust Pickering interfacial biocatalysts for efficient biotransformations and one-pot cascade reactions. *Angew. Chem. Int. Ed*. **57**, 13810–13814 (2018).

35 Schoonen, L. & van Hest, J. C. M. Compartmentalization approaches in soft matter science: from nanoreactor development to organelle mimics. Adv. Mater. 28, 1109–1128 (2016).

36 Deng, N. N., Yelleswarapu, M. & Huck, W. T. S. Monodisperse uni- and multicompartment liposomes. *J. Am. Chem. Soc*. 138, 7584–7591 (2016).

37 Jiang, H., Li, Y., Hong, L. & Ngai, T. Submicron inverse Pickering emulsions for highly efficient and recyclable enzymatic catalysis. *Chem. Asian J.* **13**, 3533–3539 (2018).

38 Zhang, Q. H., Zhang, S. G. & Deng, Y. Q. Recent advances in ionic liquid catalysis. *Green Chem*. **13**, 2619–2637 (2011).

39 Wei, L., Yan, S., Wang, H. & Yang, H. Fabrication of multi-compartmentalized mesoporous silica microspheres through a Pickering droplet strategy for enhanced CO_2 capture and catalysis. *NPG Asia Mater.* **10**, 899−911 (2018).

40 Wu, T. et al. Multi-body coalescence in Pickering emulsions. *Nat. Commun*. **6**, 5929, (2015).

41 Aveyard, R., Binks, B. P. & Clint, J. H. Emulsions stabilised solely by colloidal particles. *Adv. Colloid Interface Sci*. **100−102**, 503–546 (2003).

42 Eral, H. B., Manukyan, G. & Oh J. M. Wetting of a drop on a sphere. *Langmuir* **27**, 5340–5346 (2011).

43 Wingstrand, E., Laurell, A., Fransson, L., Hult, K. & Moberg, C. Minor enantiomer recycling: metal catalyst, organocatalyst and biocatalyst working in concert. *Chem. Eur. J*. **15**, 12107–12113 (2009).

44 Lundgren, S., Wingstrand, E., Penhoat, M. & Moberg, C. Dual Lewis acid Lewis base activation in enantioselective cyanation of aldehydes using acetyl cyanide and cyanoformate as cyanide sources. *J. Am. Chem. Soc*. **127**, 11592–11593 (2005).

45 Brunel, J. M. & Holmes, I. P. Chemically catalyzed asymmetric cyanohydrin syntheses. *Angew. Chem. Int. Ed*. **43**, 2752–2778 (2004).

46 Denard, C. A., Hartwig, J. F. & Zhao, H. M. Multistep one-pot reactions combining biocatalysts and chemical catalysts for asymmetric synthesis. *ACS Catal*. 3, 2856−2864 (2013).

47 Kim, J. H. & Kim, G. J. Enantioselectivities of chiral Ti(IV) salen complexes immobilized on MCM-41 in asymmetric trimethylsilylcyanation of benzaldehyde. *Catal. Lett.* **92**, 123–130 (2004).

48 Zhu, Y. Z., Fow, K. L., Chuah, G. K. & Jaenicke, S. Dynamic kinetic resolution of secondary

alcohols combining enzyme-catalyzed transesterification and zeolite-catalyzed racemization. *Chem. Eur. J.* 13, 541–547 (2007).

49 Lozano, P., De Diego, T., Larnicol, M., Vaultier, M. & Iborra, J. L. Chemoenzymatic dynamic kinetic resolution of *rac*-1-phenylethanol in ionic liquids and ionic liquids/supercritical carbon dioxide systems. *Biotechnol. Lett*. **28**, 1559–1565 (2006).

50 Lozano, P. et al. Long term continuous chemoenzymatic dynamic kinetic resolution of rac-1-phenylethanol using ionic liquids and supercritical carbon dioxide. *Green Chem*. 11, 538–542 (2009).

Acknowledgements

This work is supported by the Natural Science Foundation of China (21925203, 21902093 and 21733009), Program for Youth Sanjin Scholar, 100 Talent Project of Shanxi Province and the Fund for Shanxi "1331 Project".

Author contributions

H.Q.Y. conceived and supervised the project; M.Z. executed the experiments and collected the data; T.L. and L.L.D. helped M.Z. to conduct part of the experiments. N.X. contributed to preparing some of the figures. B.P.B. designed some experiments and analyzed the data. H.Q.Y. and M.Z. wrote the paper. All authors edited the paper.

Additional information

Supplementary information is available in the online version of the paper. Reprints and permissions information is available online at www.nature.com/reprints. Correspondence and requests for materials should be addressed to H.Q.Y.

Competing interests

The authors declare no competing interests.